DOI: 10.26599/FSHW.2026.9251194

Contents lists available at SciOpen

Food Science and Human Wellness

journal homepage: https://www.sciopen.com/journal/2097-0765

China Food Publishing Co.

Engineered probiotic *Escherichia coli* Nissle 1917 delivery of GPX4 suppresses pyroptosis and protects against sepsis

Hao Wang[1, †], Jinsong Zhang[2, †] Wen Li[3, †], Leyi Chu[2], Xiaofeng Ruan[2], Meng Zhou[1], Tianling Pan[2], Yue Li[2], Jinzhi Ma[2], Peng Xiao[2, *], Hong Gao[2, *]

[1] *College of Food Science and Technology, Yunnan Agricultural University, Kunming 650201, China*

[2] *College of Veterinary Medicine, Yunnan Agricultural University, Kunming 650201, China*

[3] *Faculty of Animal Science and Technology, Yunnan Agricultural University, Kunming 650201, China*

ABSTRACT: Sepsis remains a leading cause of mortality worldwide, driven by dysregulated inflammation and organ failure, with limited targeted therapies. Pyroptosis, mediated by gasdermin D (GSDMD), amplifies sepsis pathology through lipid peroxidation-dependent mechanisms, yet direct interventions are scarce. Leveraging the probiotic *Escherichia coli* Nissle 1917 (EcN) for gut-targeted delivery, we engineered EcN to secrete glutathione peroxidase 4 (GPX4), a pivotal antioxidant enzyme that curbs lipid peroxidation and pyroptosis. In an LPS-induced murine sepsis model, prophylactic oral EcN-GPX4 enhanced survival, mitigated multi-organ damage, and suppressed GSDMD cleavage across tissues. Dual mechanisms included: alleviation of oxidative stress and lipid peroxidation to block pyroptosis; and gut microbiota remodeling, enriching *Ligilactobacillus murinus*, which correlated with reduced LPS translocation and dampened arachidonic acid–linked pro-inflammatory metabolism. Via the gut–liver axis, EcN-GPX4 further attenuated hepatic TLR4/NF-κB signaling. This probiotic-based enzyme delivery offers a precise, microbiome-modulating strategy to interrupt pyroptotic amplification, with strong translational promise for sepsis management.

Keywords: *Escherichia coli* Nissle 1917; Engineered probiotic; Sepsis; Pyroptosis; GPX4; Gut-liver axis

1. Introduction

Sepsis is a critical syndrome characterized by organ dysfunction that arises from a dysregulated immune response to infection. Despite advances in supportive care and antimicrobial therapy, sepsis continues to be a predominant cause of mortality globally [1, 2]. The persistent failure of multiple immunomodulatory interventions highlights the need for mechanism-based, tissue-specific strategies that disrupt self-perpetuating inflammatory circuits without broadly suppressing immune function [3, 4]. Pyroptosis, a regulated form of lytic cell inflammatory death, has emerged as a key driver of organ injury in sepsis [5-7]. Upon inflammasome activation, inflammatory caspases cleave gasdermin D (GSDMD), which results in the release of an N-terminal fragment capable of forming membrane pores, induces cytokine release, and triggers cell lysis. This

† **Contributed equally to this work.**
***Corresponding author**
gaohongping@163.com (H.Gao).
aipengpengpiao@163.com (P.Xiao).

Received 29 September 2025
Received in revised from 29 December 2025
Accepted 12 February 2026

amplification of local and systemic inflammation contributes directly to organ dysfunction [5, 8, 9]. In both the canonical (caspase-1) and noncanonical (caspase-11/4/5) pathways, endotoxin links pathogen recognition to GSDMD-dependent membrane rupture, positioning GSDMD as a critical signaling hub in endotoxin-mediated injury [10-12].

Preclinical and translational studies show that pathological GSDMD activation not only intensifies inflammation but also promotes neutrophil extracellular trap (NET) formation and multi-organ failure, suggesting that inhibiting GSDMD-mediated pyroptosis may improve sepsis outcomes [13]. Lipid peroxidation, driven by excess reactive oxygen species (ROS) in membrane lipids, has also gained attention as a pathogenic mechanism[14, 15]. Loss of glutathione peroxidase 4 (GPX4), a key lipid-protecting antioxidant enzyme, leads to lipid ROS accumulation and worsens tissue injury [10, 16]. Evidence indicates that peroxidized membrane lipids may facilitate GSDMD pore formation and amplify pyroptotic signaling, with GPX4 acting as a key regulator of this process [10, 17]. Targeted reduction of lipid peroxidation at susceptible tissue sites may therefore inhibit GSDMD activation and prevent downstream inflammatory escalation.

The gut microbiota and the gut–liver axis are critical determinants of systemic immune regulation in sepsis. Disruption of the intestinal barrier and microbiota translocation via the portal circulation fuel hepatic inflammation and accelerate multi-organ failure [18]. The probiotic *E. coli* Nissle 1917 (EcN), a generally recognized as safe strain, exerts immunomodulatory and barrier-protective effects in intestinal disease models [19-21]. EcN has been used to enhance intestinal barrier integrity, suppress inflammation [22, 23], and, when engineered, to deliver therapeutic proteins in vivo while remodeling local immunometabolism [22, 24, 25]. Engineering EcN to locally deliver antioxidants targeting the lipid peroxidation/GSDMD axis offers a promising strategy for modulating the gut–liver–immune circuit.

Here, we engineered *E. coli* Nissle 1917 to secrete GPX4 to address a mechanistic gap in sepsis intervention: lipid peroxidation can potentiate GSDMD-dependent pyroptosis, yet in vivo strategies to restrain this coupling with spatial specificity are limited. Our study contributes: a probiotic enzyme-delivery platform enabling intestinally routed GPX4 availability; evidence that engineered EcN-GPX4 strain attenuates caspase-1 activation and GSDMD processing across gut–liver–lung in an endotoxemia model; an integrated mechanism linking redox/lipid peroxidation control to microbiota remodeling (notably enrichment of *L. murinus*) and reduced gut-derived inflammatory signaling along the gut–liver axis; and a conceptual framework for microbiome-based precision intervention targeting inflammatory cell death in sepsis.

2. Materials and methods

2.1. Construction of EcN-GPX4

The probiotic *E. coli* Nissle 1917 strain (HonorGene #HG-VDH1186) was genetically engineered using the CRISPR-Cas9 system, following established protocols [26, 27]. Competent EcN cells carrying the pCas plasmid (Addgene #62225) were prepared, confirmed by PCR (primer and sgRNA sequences listed in

Supplementary Table S1), and induced with L-arabinose (final concentration 10 mM) to activate the λ-Red recombination system.

A pUC19-glk-pHCE-pelB-GPX4 plasmid was constructed to express an sgRNA targeting the glk gene in EcN (designed using https://crispor.gi.ucsc.edu/). This plasmid also carried the mouse-derived GPX4 gene fused to a pelB signal peptide for secretory expression, driven by the pHCE promoter, and included a homologous repair template flanked by glk sequences to enable precise genomic integration of the pHCE-pelB-GPX4 cassette following CRISPR-mediated cleavage. The glk-pHCE-pelB-GPX4 sequence (Supplementary Table S2) was synthesized by Sangon Biotech and cloned into the pUC19 vector. Electroporation was performed as previously described [26]. Transformants were cultured overnight, verified by colony PCR and Sanger sequencing, and subsequently cured of the pCas plasmid according to the method of Yu Jiang et al [26].

For growth characterization, individual colonies of EcN and EcN-GPX4 were inoculated into 15 mL of LB broth and incubated overnight at 37 ℃ with agitation at 235 rpm. The following day, c the cultures were diluted at a ratio of 1:100 and incubated under identical conditions. Optical density at 600 nm was recorded at 30-minute intervals using a multifunctional microplate reader (SpectraMax M5, Molecular Devices, USA) to construct growth curves. To assess cell viability, 190 μL of overnight culture (six replicates per group) was dispensed into a 96-well plate, mixed with 10 μL CCK-8 reagent (Yeasen #40203ES), incubated at 37 ℃ for 3 hours, followed by absorbance measurement at 450 nm to assess bacterial viability.

2.2. Animal Experiments

Male C57BL/6 mice (6–7 weeks old) were obtained from the Institute of Medical Biology, Chinese Academy of Medical Sciences, and maintained in a specific-pathogen-free (SPF) facility at Yunnan Agricultural University under controlled conditions (temperature 25 ± 2 ℃; humidity 40 ± 10%; 12-h light/dark cycle) with ad libitum access to food and water.

A total of 60 mice were randomly allocated into three groups (n = 20 per group): EcN gavage, LPS treatment, and LPS + EcN co-treatment. Following a 7-day acclimatization period, the EcN and co-treatment groups received daily oral gavage of EcN suspension (2×10^9 CFU [20]) for 21 consecutive days. This dosing schedule models a prophylactic (pre-exposure). Subsequently, the LPS and co-treatment groups were administered intraperitoneal LPS (54 mg/kg [28]).

To assess the effect of EcN-GPX4, an additional treatment group (n = 20) was included, receiving the same EcN-GPX4 gavage regimen as the EcN group, followed by the same LPS dose after the final gavage. Following LPS administration, body temperature and survival were monitored, and sepsis severity was scored as described in [29].

After euthanasia, mice were dissected for macroscopic organ examination. Liver and spleen were harvested to calculate organ indices (organ weight/body weight × 100%). All procedures were approved by the Animal Ethics Committee of Yunnan Agricultural University (approval no. 202303006) and conducted in compliance with ARRIVE guidelines.

2.3. Biochemical Analysis

Blood samples were collected, and plasma was separated by centrifugation at 4 ℃. Plasma levels of AST (#C010-2-1), ALT (#C009-2-1), BUN (#C013-2-1), and Scr (#C011-2-1) were measured using commercial kits from Nanjing Jiancheng Bioengineering Institute, following the manufacturer's instructions, to evaluate hepatic and renal function. Mouse-specific ELISA kits were used to quantify plasma cytokines, including IL-18 (Jonln #JLW20253), IL-1α (#JL13044), IL-3 (#JL20261), and TNF-α (#JLW10484). LPS levels in serum and liver tissues were determined using mouse LPS ELISA kits (#JL20691).

2.4. Histological Analysis

Tissues were fixed in 4% paraformaldehyde, dehydrated through a graded ethanol series, and embedded in paraffin. Sections (5 μm) were deparaffinized, rehydrated, and stained with hematoxylin and eosin (H&E) for microscopic examination using an Olympus BX53 light microscope.

For immunohistochemistry (IHC), tissue sections were deparaffinized and subjected to heat-mediated antigen retrieval in citrate buffer. Endogenous peroxidase activity was suppressed using hydrogen peroxide, and nonspecific binding sites were blocked with 5% BSA. The slides were incubated overnight at 4 ℃ with an IL-1β primary antibody (Proteintech, #16806-1-AP), followed by incubation with a secondary antibody at room temperature for 1.5 hour. Visualization was achieved using a streptavidin–biotin–peroxidase complex and DAB substrate, counterstained with hematoxylin, and examined microscopically.

2.5. Immunofluorescence Assay (IF)

Antigen retrieval of intestinal tissue sections was conducted using the eBioscience™ IHC kit (Thermo Fisher Scientific) according to the manufacturer's instructions. Tissue sections and cell slides were subsequently blocked with 5% BSA for 0.5 hour, followed by incubation with primary antibodies against NLRP3 (Proteintech, #60127-1) and Caspase-1 (Proteintech, #66826-1). Fluorescently labeled secondary antibodies were then applied, and nuclei were counterstained with DAPI.

2.6. qPCR

Total RNA was isolated using the TRIzol RNA (Thermofisher #15596026) and reverse-transcribed into cDNA with PrimeScript™ RT reagent Kit (TAKARA, #RR037Q). GAPDH was employed as the internal reference gene. qPCR was conducted using the TB Green® Premix Ex Taq™ II (TAKARA, #RR820Q). Primer sequences were designed according to the PrimerBank database [30, 31]. Relative gene expression levels were determined using the 2-ΔΔCt method.

2.7. Western blot

Proteins were extracted using RIPA lysis buffer, quantified by the BCA assay, separated on 12% SDS-PAGE gels, and transferred onto PVDF membranes. The membranes were blocked for 15minutes and subsequently incubated overnight at 4 ℃ with primary antibodies against Caspase-1 (Abcam, #ab207802),

GSDMD (Abcam, #ab209845), TLR4 (Proteintech, #19811-1-AP), NF-κB (Proteintech, #10745-1-AP), p-p65 (Proteintech, #82335-1-RR), MyD88 (Proteintech, #23230-1-AP), and GPX4 (Proteintech, #67763-1-IG). After washing with TBST, the membranes were incubated with HRP-conjugated secondary antibodies for 90 minutes. Protein bands were detected using a chemiluminescence method. GAPDH (Proteintech, #60004-1-AP) was used as the loading control.

2.8. Transcriptomic Analysis of Sepsis Samples

The MINiML-format dataset (GSE100159) was downloaded from the GEO database and normalized using the normalize. quantiles function in the preprocessCore R package. Differentially expressed genes were identified with the limma package (v4.2.2), applying thresholds of adjusted $P < 0.05$ and $|\log_2 FC| > 1$. Functional enrichment was assessed via KEGG pathway analysis.

2.9. Gut Microbiota Diversity Analysis

Microbial DNA was extracted from colonic contents using the QIAamp DNA Stool Mini Kit. Libraries were prepared and sequenced on the Illumina NovaSeq platform (Biomker Technologies, Shanghai). Analyses included alpha and beta diversity metrics, LEfSe analysis (LDA > 4, $P < 0.05$) to identify differential taxa, and KEGG pathway prediction using PICRUSt.

2.10. Metabolomics Analysis

Non-targeted metabolomics of mouse liver samples was performed using a Waters Acquity I-Class PLUS UHPLC system coupled to a Waters Xevo G2-XS QTOF mass spectrometer. Samples were extracted, centrifuged, and supernatants analyzed by LC-MS in both positive and negative ion modes on a Q-Exactive HF-X system (Biomker Technologies). Metabolites were annotated via the HMDB database, retaining only features with RSD < 30%. Multivariate analyses (PCA, PLS-DA) were conducted with SIMCA-P software, and differential metabolites were selected using VIP > 1, $P < 0.05$. False discovery rate (FDR) was controlled for metabolomics using a standard multiple-testing correction approach (Benjamini–Hochberg)

2.11. Molecular Docking

Crystal structures of GSDMD (PDB: 5NH1) and GPX4 (PDB: 2GS3) were retrieved from the RCSB PDB database. Protein–ligand docking was performed using the HDOCK SERVER (http://hdock.phys.hust.edu.cn/). Docking scores near −200, together with confidence levels > 0.7, were considered indicative of high binding probability [32].

2.12. Statistical Analysis

All experiments were repeated independently at least three times. Data are presented as mean ± SEM. For comparisons between two groups, an unpaired two-tailed Student's t-test was used. For experiments involving more than two groups, two-way ANOVA was applied followed by an appropriate post-hoc multiple-

comparison procedure (Tukey's test) to control family-wise error. Survival was analyzed by the Kaplan–Meier method and compared using the log-rank test. A P value < 0.05 was considered statistically significant."

3. Result

3.1. Oral Administration of Probiotic EcN Alleviates Sepsis-Induced Damage

To evaluate the protective effects of EcN in sepsis, a murine sepsis model was established via LPS injection, with oral EcN administered for 21 consecutive days prior to induction (Fig. 1A). Following LPS challenge, mice exhibited a rapid decline in body temperature. A similar pattern was observed in the EcN-pretreated group; however, in these mice, temperature began to recover approximately 9 hours after injection and gradually returned to baseline (Fig. 1B).

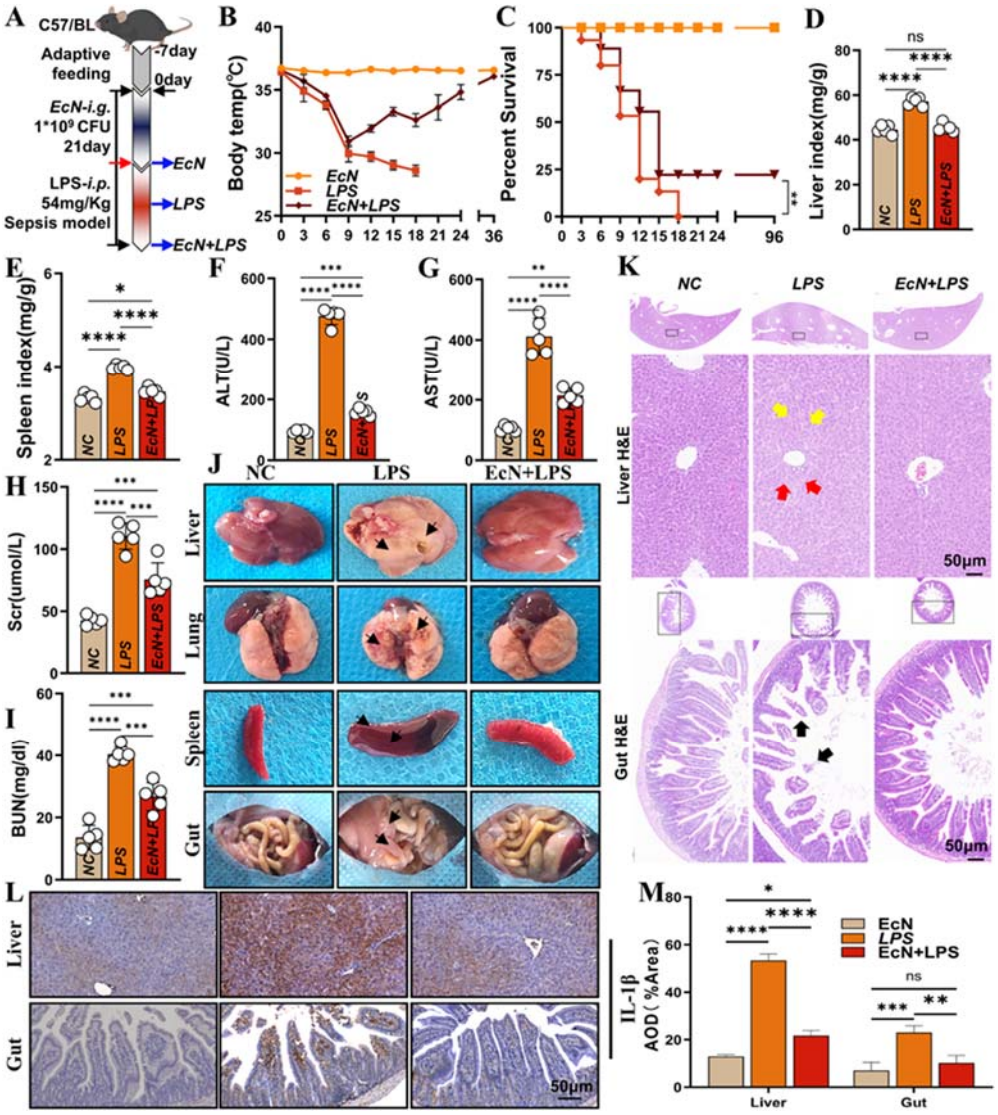

Fig. 1. Oral administration of probiotic EcN alleviates sepsis-induced multi-organ injury. (A) Schematic of sepsis model design, showing EcN intervention and LPS induction procedures; (B–C) Changes in body temperature and survival curves of mice in each group (n = 20); (D–E) Organ indices of liver and spleen (n = 5); (F–I) Serum levels of (F) ALT, (G) AST, (H) Scr, and (I) BUN (n = 5); (J) Gross morphological examination of liver, lung, spleen, and intestine; (K) H&E staining of liver and intestinal tissues (scale bar: 50 μm; red arrows, hepatocyte death/nuclear loss; blue arrows, disorganization of hepatic cords; black arrows, destruction of intestinal villi); (L–M) Immunohistochemical staining of IL-1β in liver and intestinal tissues (scale bar: 50 μm). Data are presented as mean ± SEM (two-way ANOVA). *P < 0.05, **P < 0.01, ***P < 0.001, ****P < 0.0001.

Survival analysis showed that EcN pretreatment significantly improved survival in septic mice (Fig. 1C). EcN administration also reduced LPS-induced hepatosplenomegaly (Fig. 1D–E) and markedly improved liver and kidney function, as evidenced by reduced serum levels of AST, ALT, BUN, and Scr (Fig. 1F–I). Gross anatomical examination revealed that EcN alleviated visible sepsis-related damage to the liver, lungs, spleen, and intestines (Fig. 1J). Histological evaluation further confirmed that EcN mitigated hepatocyte death, preserved hepatic cord organization, and protected against intestinal epithelial cell injury and villus structural damage (Fig. 1K). Moreover, EcN markedly reduced IL-1β expression in both liver and intestinal tissues, suggesting an attenuation of the systemic inflammatory response (Fig. 1L–M). Collectively, these findings demonstrate that prophylactic oral EcN administration prior to sepsis induction can effectively reduce multi-organ injury and inflammation caused by sepsis.

3.2. EcN Mitigates Sepsis via Casp1–GSDMD-Regulated Pyroptosis

Transcriptomic profiling of sepsis samples revealed substantial enrichment of the NOD-like receptor signaling pathway, indicating its prominent role in sepsis progression (Fig. 2A). Further gene-level analysis showed increased expression of Caspase-1 and GSDMD (Fig. 2B–C). In line with these findings, our septic mouse model displayed markedly elevated mRNA levels of NLRP3 inflammasome-associated components (NLRP3, Caspase-1, GSDMD, ASC, and IL-1β), whereas EcN pretreatment effectively suppressed their expression (Fig. 2D). Previous studies have demonstrated that activation of the NOD inflammasome drives cleavage of pro-Casp-1 into its active form, which subsequently cleaves GSDMD to generate GSDMD-N, a key effector that triggers pyroptotic cell death [33-35]. Based on this mechanism, we examined Casp-1 activation and GSDMD processing in septic mice. Western blot analysis demonstrated pronounced Casp-1 activation and GSDMD cleavage following LPS challenge, both of which were attenuated by EcN treatment. Importantly, these inhibitory effects were evident in intestinal, hepatic, and pulmonary tissues (Fig. 2E–F). Taken together, these results suggest that Casp-1–GSDMD-dependent pyroptosis is a critical mediator of sepsis pathogenesis, and that EcN confers protection against sepsis-induced organ injury primarily by suppressing this pathway.

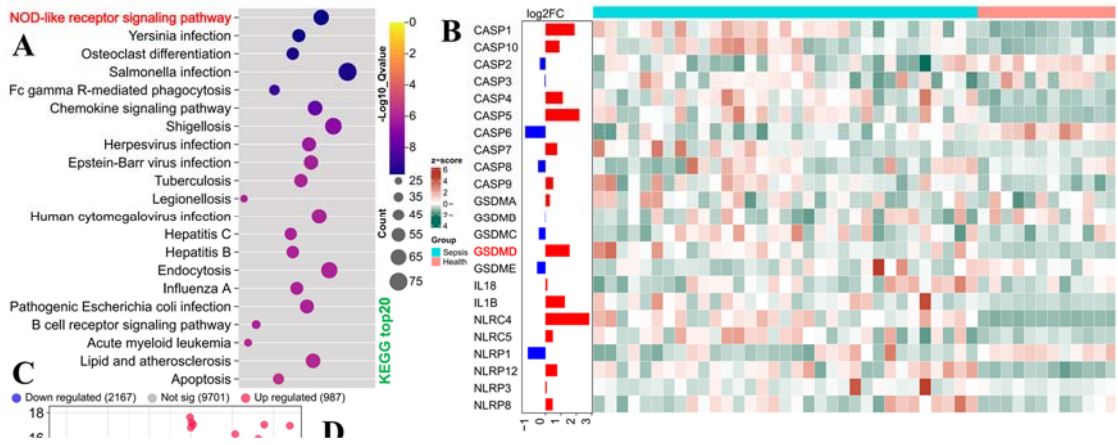

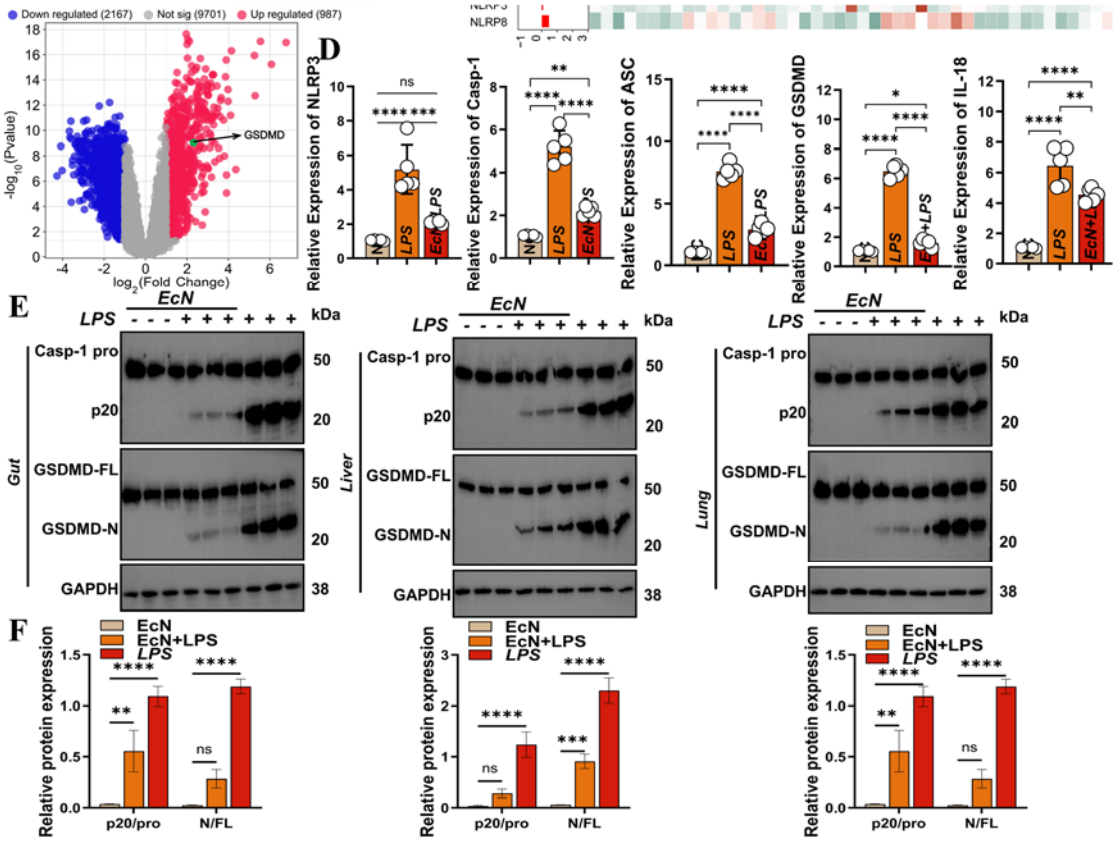

Fig. 2. EcN mitigates sepsis injury by inhibiting Casp1–GSDMD-mediated pyroptosis. (A) KEGG enrichment analysis of differentially expressed genes in sepsis, highlighting significant pathways such as the NOD-like receptor signaling pathway; (B) Hierarchical clustering heatmap of differential genes within the NOD-like receptor signaling pathway; (C) Volcano plot of differential genes (red, upregulated; blue, downregulated; pyroptosis-related genes labeled); (D) Hepatic mRNA expression levels of NLRP3 inflammasome–related genes (NLRP3, Caspase-1, ASC, GSDMD, and IL-1β) (n = 5); (E–F) Western blot analysis of Caspase-1 activation and GSDMD cleavage in intestinal, hepatic, and pulmonary tissues. Data are presented as mean ± SEM. (two-way ANOVA). * $P < 0.05$, ** $P < 0.01$, *** $P < 0.001$, **** $P < 0.0001$.

3.3. Genetic Engineering Enhances the Anti-inflammatory Activity of EcN

Transcriptomic analysis of sepsis samples revealed significant enrichment of pathways related to oxidative stress and inflammation, including ROS metabolic processes, responses to oxidative stress, NF-κB signaling, and Toll-like receptor signaling (Fig. 3A). GPX4 is a key antioxidant enzyme that maintains intracellular redox homeostasis by reducing lipid hydroperoxides and plays a crucial role in regulating oxidative stress and inflammatory responses [36-38]. To harness this potential, we engineered an EcN strain capable of delivering GPX4. The murine GPX4 sequence, driven by the pHCE promoter and fused with the pelB secretion signal peptide, was cloned into a pUC19-glk plasmid containing an sgRNA targeting the glk gene, thereby generating the recombinant plasmid pUC19-glk-pHCE-pelB-GPX4 (Fig. 3B–C). This plasmid was integrated into the glk locus of the EcN genome via homologous recombination (Fig. 3D). PCR verification confirmed pCas plasmid-containing EcN strains (Fig. S1A), and subsequent PCR and sequencing validated the correct insertion of pHCE-pelB-GPX4 into the EcN genome (Fig. S1B). The engineered strain was designated EcN-GPX4.

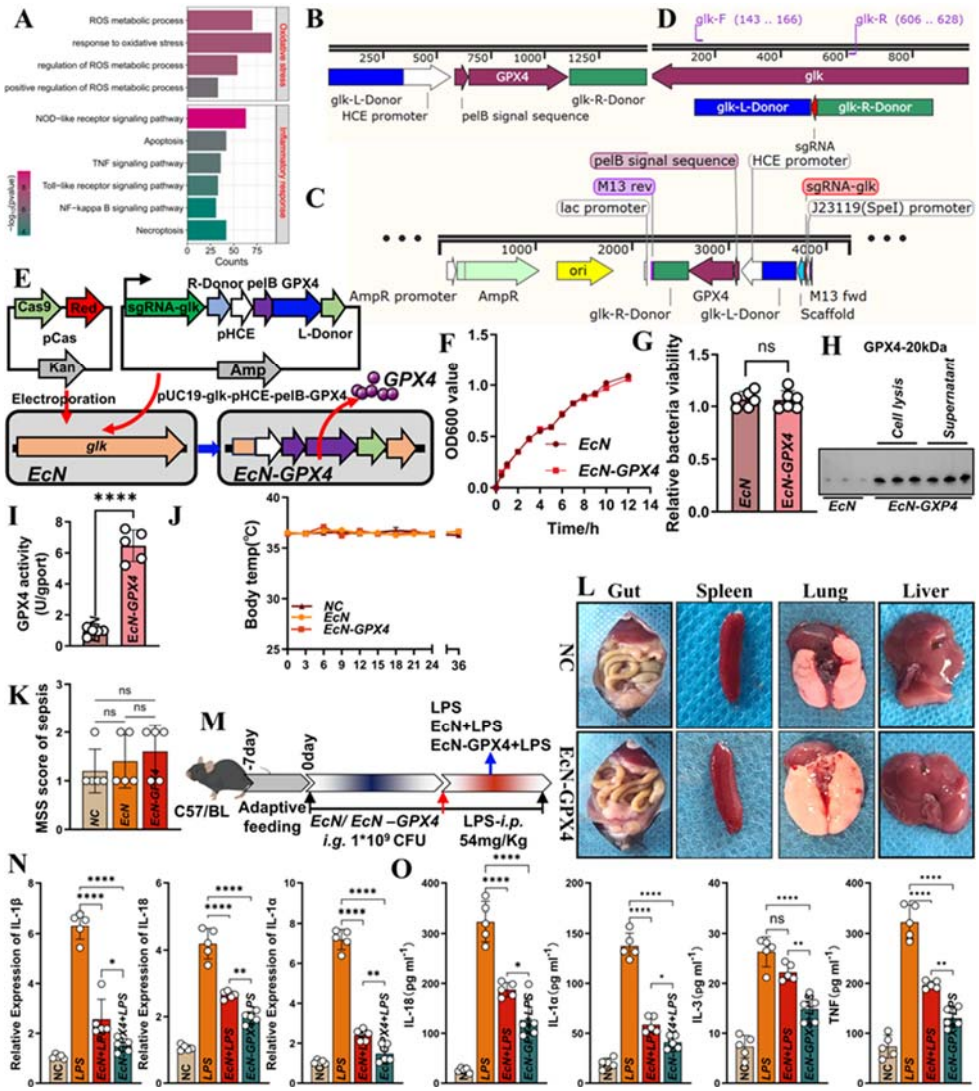

Fig. 3. Genetic engineering enhances the anti-inflammatory activity of EcN. (A) GO functional enrichment analysis of differentially expressed genes, including terms related to oxidative stress and inflammatory responses; (B) Structure of the pHCE-pelB-GPX4 sequence, showing the HCE promoter, pelB signal peptide, GPX4 coding region, and glk homologous arms; (C) Map of recombinant plasmid pUC19-glk-pHCE-pelB-GPX4; (D) Schematic of integration into the glk locus of the EcN genome; (E) Construction workflow of EcN-GPX4 engineered strain; (F–G) Growth curve and viability assay of the engineered strain; (H) Western blot detection of GPX4 expression in bacterial lysates and supernatants; (I) Comparison of GPX4 enzymatic activity between EcN and EcN-GPX4 (n = 5); (J–L) Safety evaluation of EcN-GPX4, including changes in body temperature, clinical scores, and gross morphology of liver, lung, spleen, and intestine; (M) Experimental design for EcN-GPX4 intervention in sepsis model; (N) Hepatic mRNA expression of inflammatory cytokines IL-18, IL-1α, and IL-1β (n = 5); (O) Serum levels of IL-1α, IL-18, IL-3, and TNF-α (n = 5). Data are presented as mean ± SEM. (two-way ANOVA). * $P < 0.05$, ** $P < 0.01$, *** $P < 0.001$, **** $P < 0.0001$.

Growth kinetics showed no significant differences in growth rate or viability between EcN-GPX4 and wild-type EcN (Fig. 3F–G). GPX4 expression was detected in both cell lysates and culture supernatants of EcN-GPX4, and the enzyme exhibited strong activity (Fig. 3H–I). Safety assessments demonstrated that oral EcN-GPX4 administration did not alter body temperature, clinical scores, or organ morphology in mice (Fig. 3J–L). In a murine sepsis model, EcN-GPX4 outperformed wild-type EcN, more effectively reducing hepatic pro-inflammatory cytokines (IL-1α, IL-1β, IL-18) (Fig. 3N) and attenuating systemic cytokine storm manifestations, as evidenced by lower serum IL-1α, IL-3, IL-18, and TNF-α levels (Fig. 3O). Collectively, these findings confirm the successful construction of EcN-GPX4, which exhibits superior anti-inflammatory activity compared with wild-type EcN.

3.4. EcN-GPX4 Remodels the Gut Microbiota to Alleviate Intestinal Inflammatory Injury

Previous studies have shown that LPS can exacerbate tissue injury by disrupting the composition and function of the gut microbiota [39, 40]. To explore the impact of EcN-GPX4 on gut microbiota during the regulation of inflammatory responses, we compared microbial diversity and composition in mice pretreated with EcN or EcN-GPX4 prior to LPS exposure. PCoA analysis revealed distinct clustering between the two groups, indicating significant compositional differences (Fig. 4A). FAPROTAX-based functional annotation showed that EcN-GPX4 pretreatment markedly reduced the enrichment of LPS-induced microbes associated with "human_pathogens_all" and "human_pathogens_gastroenteritis" (Fig. 4B). LEfSe analysis further revealed a significantly higher abundance of *Ligilactobacillus* and *Ligilactobacillus_murinus* (*L. murinus*) (a potential probiotic [41, 42]) in the EcN-GPX4 group compared with the EcN group (Fig. 4C). Notably, taxonomic profiling demonstrated consistent increases in *Ligilactobacillus* abundance across multiple taxonomic ranks (phylum, order, family, and genus) in the EcN-GPX4 group (Fig. 4D–G), with species-level analyses confirming the enrichment of *L. murinus* (Fig. 4H). Microbial interaction network analysis indicated that *L. murinus* occupied a key network node in the EcN-GPX4 group, suggesting a pivotal role in maintaining microbial homeostasis and mitigating sepsis-associated injury (Fig. 4I).

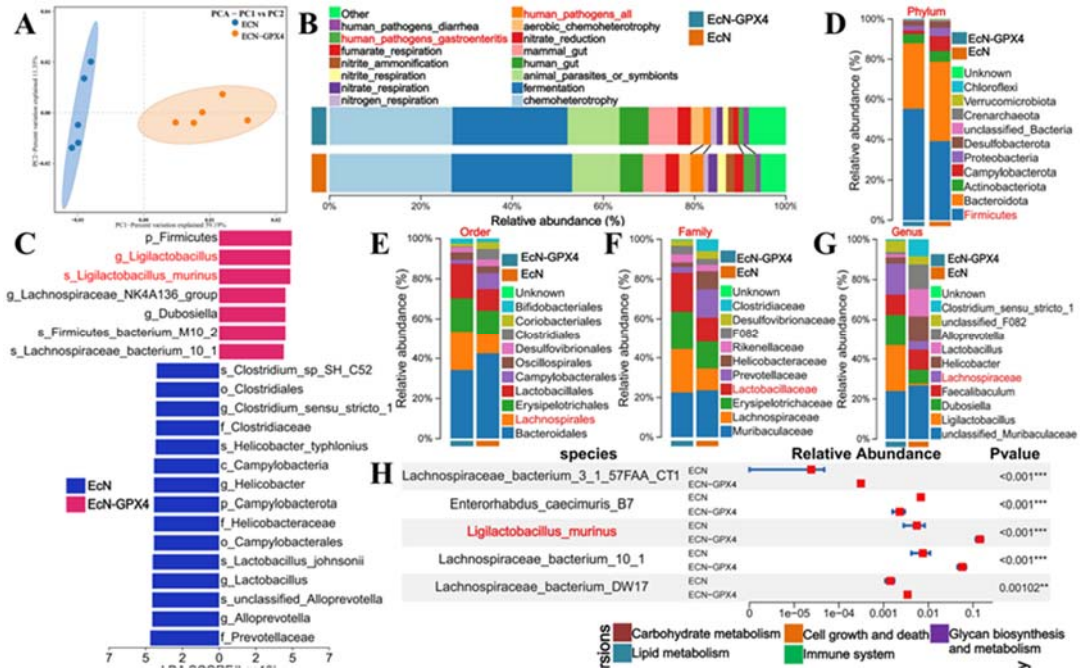

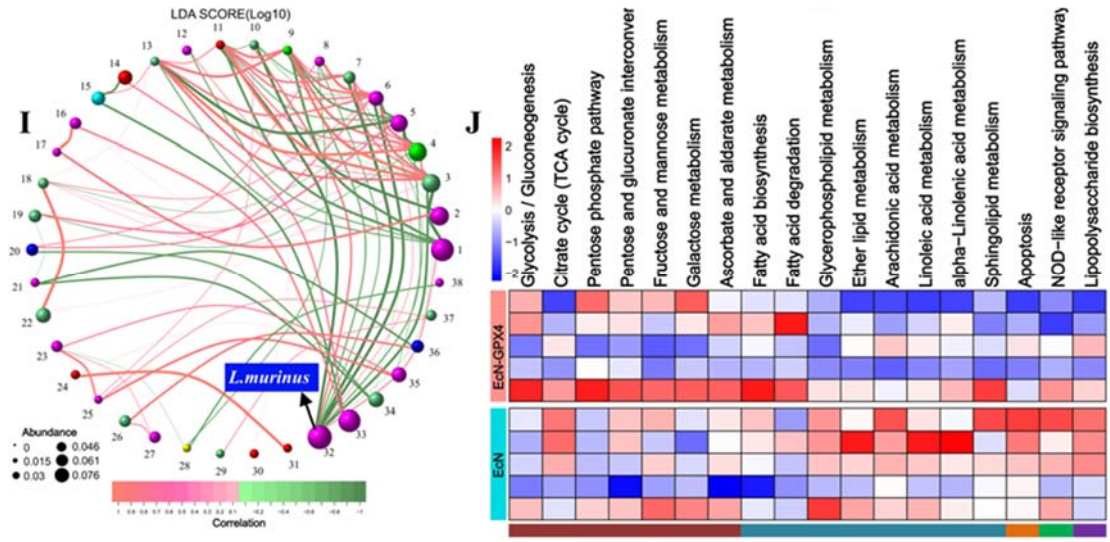

Fig. 4. Gut microbiota diversity analysis in EcN-GPX4–treated mice. (A) PCoA based on Bray–Curtis distance illustrating differences in microbial community structure between groups; (B) Functional annotation of differential taxa via FAPROTAX; (C) LEfSe analysis (LDA score plot) comparing groups; (D–H) Relative abundance of differential taxa at phylum, order, family, genus, and species levels; (I) Spearman correlation–based microbial co-occurrence network; (J) PICRUSt2 functional predictions comparing microbial enrichment in lipid peroxidation– and inflammation-related pathways among groups.

PICRUSt2 functional predictions of differential taxa indicated that EcN-GPX4 reduced microbial metabolic pathways related to lipid peroxidation (e.g., arachidonic acid metabolism, alpha-linolenic acid metabolism, and linoleic acid metabolism) and suppressed the inflammation-associated NOD-like receptor signaling pathway (Fig. 4J). We then assessed the activation state of the canonical inflammatory signaling pathway TLR4/NF-κB in the gut [43]. Results showed that LPS activated the TLR4/NF-κB pathway, whereas EcN-GPX4 pretreatment suppressed its activation more effectively than EcN (Fig. 5A–B), concomitantly reducing intestinal IL-1β expression (Fig. 5C–D). Moreover, EcN-GPX4 significantly inhibited assembly of the NLRP3 inflammasome in the gut compared with EcN (Fig. 5E). Taken together, these findings suggest that EcN-GPX4 alleviates LPS-induced intestinal injury by remodeling the gut microbiota, promoting the expansion of beneficial taxa such as *L. murinus*, and suppressing intestinal inflammatory signaling pathways.

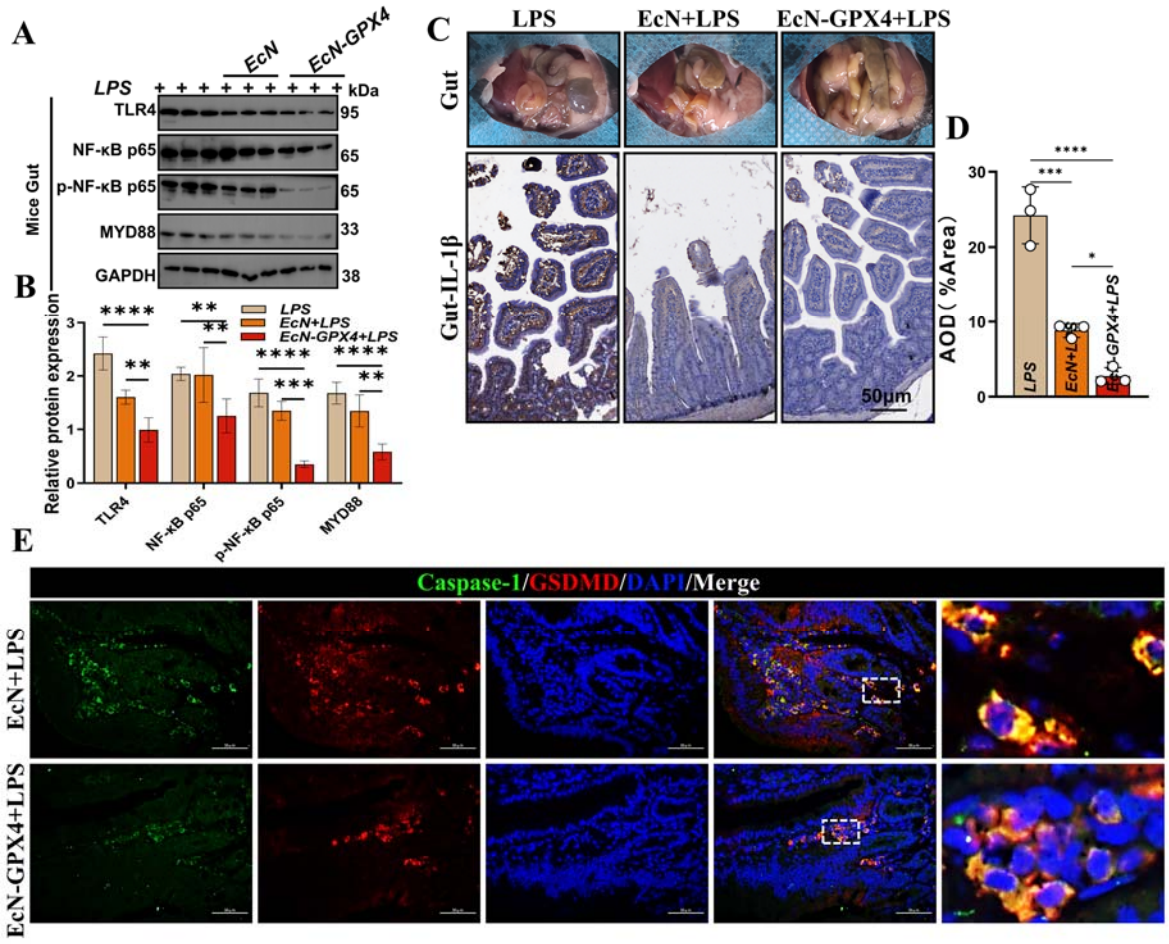

Fig. 5. EcN-GPX4 improves gut microbiota composition to alleviate intestinal inflammatory injury. (A–B) Western blot analysis of intestinal TLR4/NF-κB pathway–related proteins (TLR4, NF-κB, p-NF-κB, MyD88); (C–D) Gross morphology of intestines and immunohistochemical staining of IL-1β in intestinal sections (scale bar: 50 μm); (E) Immunofluorescence imaging of NLRP3 inflammasome assembly in intestines from different treatment groups (scale bar: 50 μm; green, Caspase-1; red, NLRP3; blue, DAPI). Data are presented as mean ± SEM. (two-way ANOVA). * $P < 0.05$, ** $P < 0.01$, *** $P < 0.001$, **** $P < 0.0001$.

3.5. EcN-GPX4 Alleviates Lipid Peroxidation to Block GSDMD Activation and Pyroptosis

Previous studies have shown that GPX4 can inhibit GSDMD cleavage during inflammasome activation, while oxidative stress induced lipid peroxidation promotes GSDMD-N–mediated pyroptosis [10]. To interrogate whether EcN-GPX4 is associated with altered oxidative lipid metabolism during sepsis, we performed untargeted liver metabolomic profiling in septic mice pretreated with EcN or EcN-GPX4. PCA revealed a clear separation in metabolic profiles between the two groups (Fig. 6A). Differential metabolite analysis identified 1,496 upregulated and 1,486 downregulated metabolites in the EcN-GPX4 group relative to EcN controls (Fig. 6B), and hierarchical clustering confirmed that EcN-GPX4 reshaped the hepatic metabolic landscape (Fig. 6C). KEGG annotation of differential metabolites revealed significant enrichment in lipid metabolism pathways (Fig. 6D), particularly arachidonic acid metabolism, which is closely associated with lipid peroxidation [44]. Functional enrichment analysis further indicated involvement of classical oxidative stress and lipid peroxidation related pathways, including reactive oxygen species metabolism, glutathione metabolism, linoleic, α-linolenic, and arachidonic acid metabolism, as well as ferroptosis. Notably,

EcN-GPX4-induced metabolic shifts were also associated with suppression of the inflammatory NOD-like receptor signaling pathway (Fig. 6D).

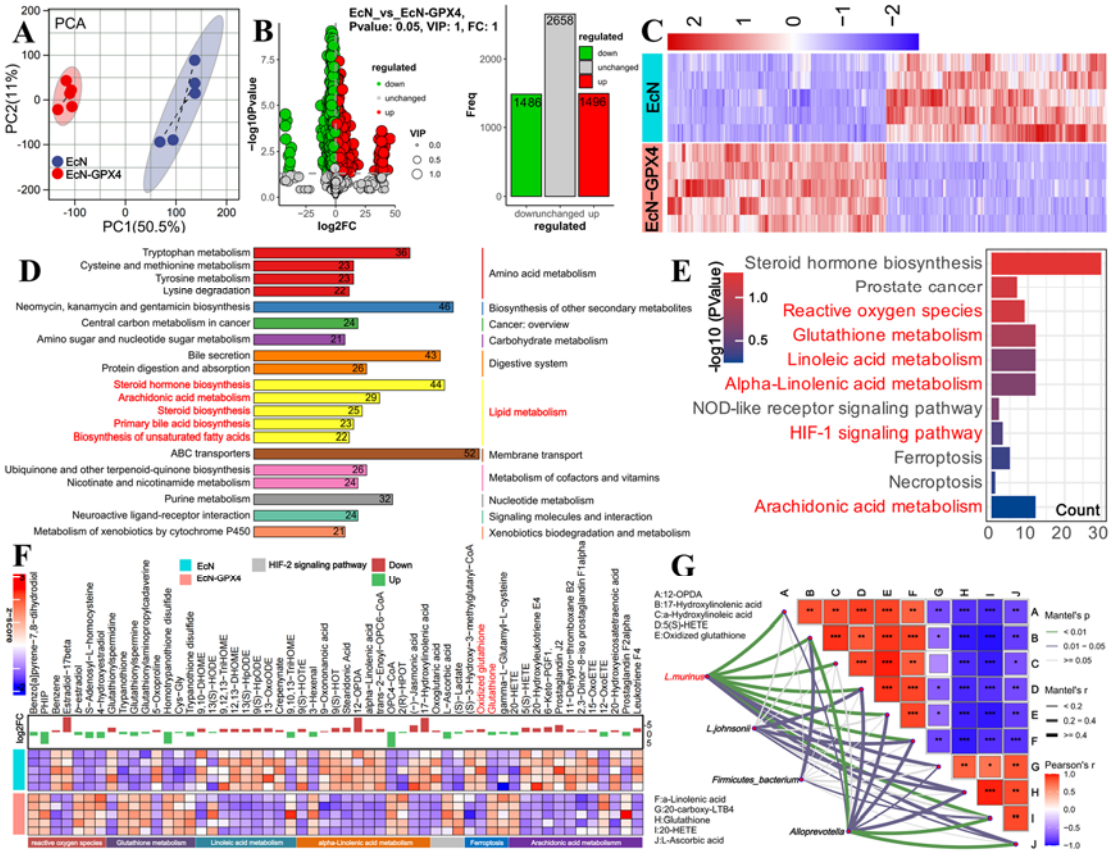

Fig. 6. EcN-GPX4 alleviates lipid peroxidation during sepsis. (A) PCA showing distinct metabolite profiles between groups; (B) Volcano plot and statistical summary of differential metabolites; (C) Heatmap of hepatic metabolites in EcN- and EcN-GPX4-pretreated mice; (D–E) KEGG enrichment analysis of differential metabolites, highlighting oxidative stress– and lipid peroxidation–related pathways, including lipid metabolism, reactive oxygen species metabolism, and arachidonic acid metabolism; (F) Clustering of differential metabolites related to oxidative stress and lipid peroxidation; (G) Correlations between lipid peroxidation–related metabolites and four microbial species: shading represents Pearson correlation coefficients; Mantel test used to evaluate microbe–metabolite associations.

Metabolite clustering revealed that EcN-GPX4 increased levels of antioxidants and lipid peroxidation inhibitors (e.g., glutathione, L-ascorbic acid) while reducing pro-oxidative metabolites (e.g., oxidized glutathione, 17-hydroxylinolenic acid, α-hydroxylinoleic acid) [45]. Correlation analysis showed that these beneficial metabolic changes were closely associated with Ligilactobacillus murinus abundance. Together, these results suggest that EcN-GPX4 reprograms host metabolism to alleviate oxidative stress-driven lipid peroxidation during sepsis, with effects that may involve *L. murinus*.

To determine whether these changes influence pyroptosis, we assessed pyroptosis-related protein expression in septic mice treated with EcN or EcN-GPX4. Western blot analysis revealed that EcN-GPX4 more effectively inhibited Caspase-1 activation and GSDMD cleavage than EcN, thereby blocking pyroptosis in intestinal, hepatic, and pulmonary tissues (Fig. 7A–B). Molecular docking simulations suggested possible direct interaction between GPX4 and GSDMD (Fig. 7C, Table S3). EcN-GPX4 also lowered clinical severity scores (Fig. 7D) and, importantly, further improved survival rates beyond those achieved with EcN (Fig. 7D).

Collectively, these findings indicate that EcN-GPX4 enhances survival in sepsis by reducing lipid peroxidation, inhibiting GSDMD activation, and preventing pyroptosis.

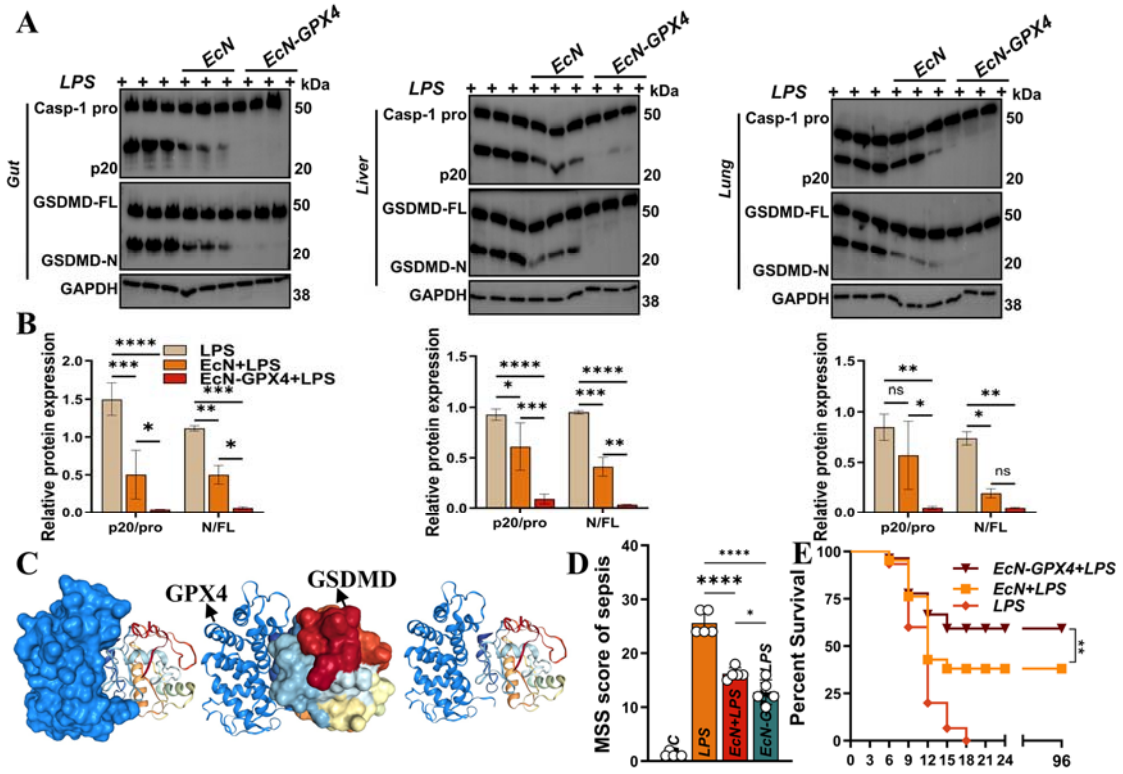

Fig. 7. EcN-GPX4 blocks GSDMD activation and pyroptosis. (A–B) Western blot detection of Caspase-1 activation and GSDMD cleavage in intestinal, hepatic, and pulmonary tissues; (C) Molecular docking simulation of GPX4 interaction with GSDMD; (D) Clinical scores of septic mice in each group (n = 5); (E) Kaplan–Meier survival curves of mice receiving different treatments (n = 20). Data are presented as mean ± SEM. (two-way ANOVA). * $P < 0.05$, ** $P < 0.01$, *** $P < 0.001$, **** $P < 0.0001$.

3.6. EcN-GPX4 Attenuates Hepatic Inflammation via the Gut–LPS–Liver Axis

We found that both EcN and EcN-GPX4 significantly reduced LPS levels in the blood and liver of septic mice (Fig. 8A–B). Gut-derived signals are key regulators of systemic inflammation, and the gut–liver axis can exacerbate hepatic injury and promote multi-organ failure via barrier disruption and microbial translocation [18]. Correlation analysis revealed a negative association between *L. murinus* abundance and LPS levels in both blood and liver (Fig. 8C). Additionally, LPS concentrations were negatively correlated with the metabolite 12-OPDA (Fig. 8D), a lipid-derived anti-inflammatory mediator known to inhibit LPS-induced NF-κB activation [46].

Based on these observations, we examined TLR4/NF-κB pathway activation in the liver. Compared with EcN, EcN-GPX4 more strongly suppressed hepatic TLR4/NF-κB activation (Fig. 8E). EcN-GPX4 also reduced hepatomegaly, ameliorated histological liver injury, decreased IL-1β expression (Fig. 8F–G), and significantly lowered serum AST and ALT levels (Fig. 8F,H), indicating improved hepatic function. Microbiota correlation analysis suggested that these protective effects were closely linked to *L. murinus* enrichment (Fig. 8C). Collectively, these findings support that EcN-GPX4 alleviates hepatic inflammation in sepsis by modulating the Gut–LPS–Liver axis.

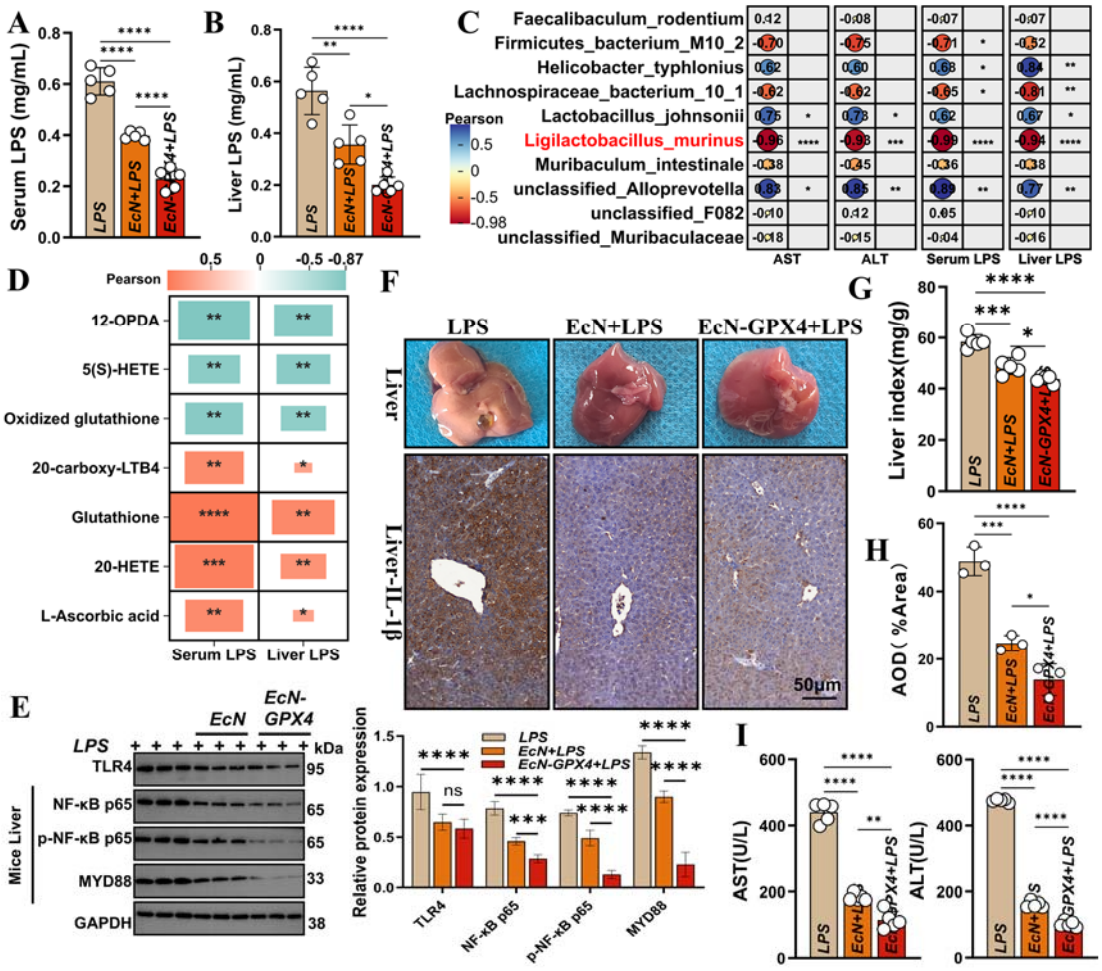

Fig. 8. EcN-GPX4 alleviates hepatic inflammation through the Gut–LPS–Liver axis. (A–B) LPS levels in serum and liver from mice after different treatments (n = 5); (C) Correlation analysis between differential taxa and LPS levels in serum and liver, as well as liver injury indices (AST, ALT); (D) Correlation analysis between lipid peroxidation–related differential metabolites and LPS levels in serum and liver; (E) Western blot detection of hepatic TLR4/NF-κB pathway–related proteins (TLR4, NF-κB, p-NF-κB, MyD88); (F) Gross liver morphology and IL-1β immunohistochemistry in liver sections (scale bar: 50 μm); (G) Liver index in each group (n = 5); (H) Quantitative analysis of IL-1β immunohistochemistry corresponding to panel (F); (I) Serum AST and ALT levels in each group (n = 5). Data are presented as mean ± SEM. (two-way ANOVA). * $P < 0.05$, ** $P < 0.01$, *** $P < 0.001$, **** $P < 0.0001$.

4. Discussion

This study presents and validates an oral GPX4 delivery strategy using an engineered probiotic strain, EcN-GPX4. The strain efficiently delivers GPX4, enabling suppression of lipid peroxidation and GSDMD-dependent pyroptosis, remodeling of beneficial gut microbiota, and attenuation of hepatic inflammation via the gut–LPS–liver axis. These combined effects significantly improved survival in septic mice, supporting a novel microbiota-targeted intervention. The protective mechanisms are primarily: probiotic GPX4 delivery dampens lipid peroxidation to restrain GSDMD-dependent pyroptosis, while microbiota remodeling associates with reduced gut-derived LPS burden and attenuated inflammatory signaling along the gut–liver axis (Fig. 9).

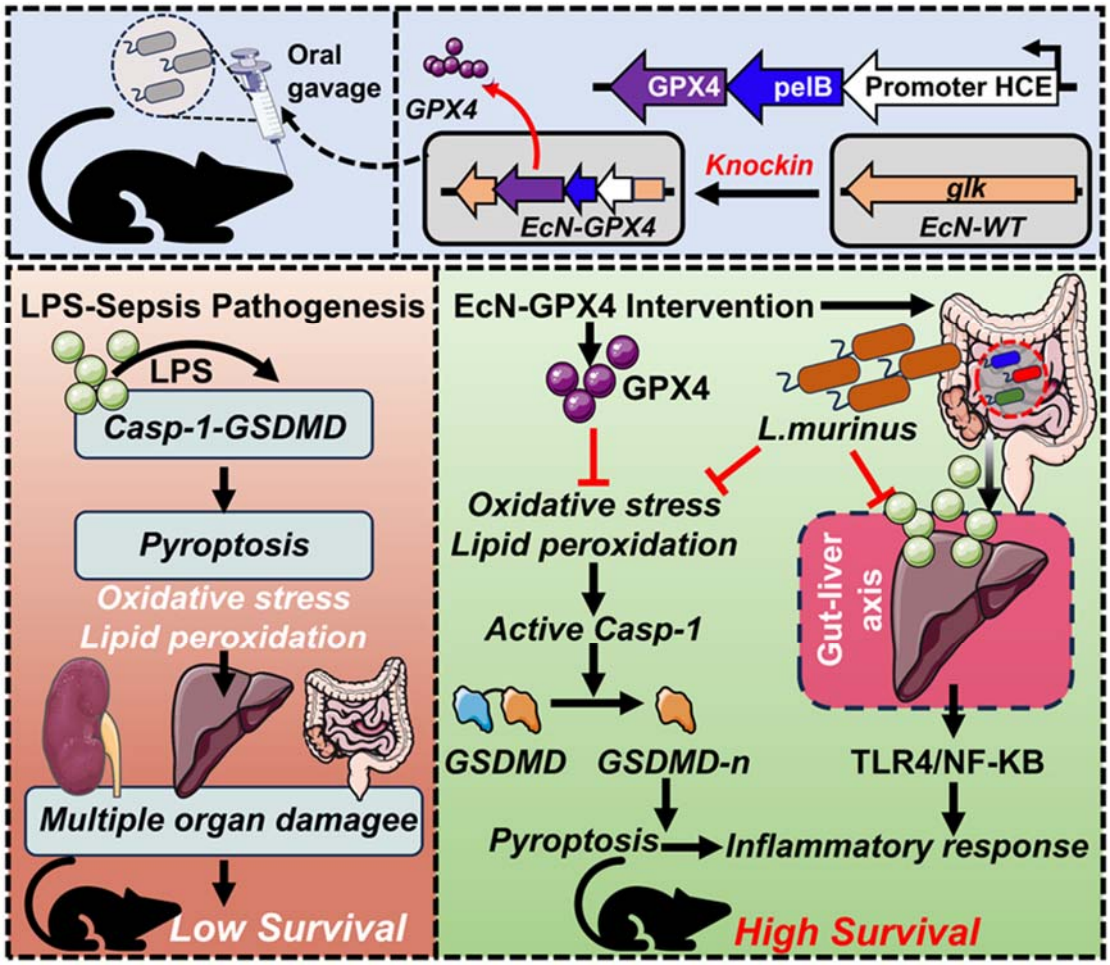

Fig. 9. Schematic overview of EcN-GPX4 mechanisms in sepsis, depicting GPX4 delivery reducing lipid peroxidation and GSDMD-pyroptosis, microbiota remodeling, and gut–liver axis modulation to suppress hepatic inflammation.

Liver metabolomics revealed decreased pro-oxidative metabolites, such as oxidized glutathione, and increased antioxidants including glutathione and L-ascorbic acid. GPX4 delivery also modulated host metabolism, suppressing arachidonic acid related pro-inflammatory pathways. Mechanistically, GPX4 inhibits lipid peroxidation, directly preventing GSDMD cleavage and pyroptosis across multiple organs. Consistent with prior reports, lipid peroxidation promotes GSDMD oligomerization and pore formation [10]. Our findings extend this by demonstrating that localized, probiotic-mediated GPX4 delivery confers tissue-specific anti-lipid peroxidation effects. EcN-GPX4 exhibited markedly stronger intervention efficacy than wild-type EcN, underscoring the importance of targeted enzymatic suppression of lipid peroxidation, consistent with evidence linking GPX4 deficiency to worsened pyroptosis in sepsis [10, 47]. Unlike genetic or systemic pharmacological activation, this probiotic delivery platform may offer greater intestinal specificity and reduced off-target effects.

A key unresolved issue is whether the protective phenotype is driven predominantly by bacteria-derived GPX4 activity or by secondary modulation of host GPX4 signaling. In the current study, GPX4 was detected in engineered EcN lysates and supernatants, supporting extracellular availability, but we did not directly quantify GPX4 uptake by host cells or changes in tissue GPX4 abundance. Future studies using tissue-specific GPX4 loss-of-function models and/or pharmacological GPX4 inhibition, together with fluorescently tagged

GPX4 tracking, will be important to dissect bacterial versus host contributions and to determine whether secreted GPX4 is internalized or acts primarily via local antioxidative buffering. In addition, colonization persistence and clearance kinetics of EcN-GPX4 were not measured, and the in vivo stability/half-life of secreted GPX4 remains to be defined. These parameters will be critical for dosing optimization and biosafety evaluation, and can be addressed by longitudinal fecal shedding quantification (CFU/qPCR), plasmid/genomic stability assays, and in situ GPX4 activity measurements along the gastrointestinal tract.

Beyond its enzymatic activity, EcN-GPX4 reshaped the gut microbiota, notably enriching *L. murinus*. This enrichment was closely associated with reduced LPS translocation and suppression of hepatic TLR4/NF-κB activation. Prior studies have reported that *L. murinus* can work synergistically with other probiotics to inhibit macrophage pyroptosis via the butyrate/GPR109A/GSDMD axis [41], this aligns with our conclusion. Importantly, our current data are associative; causal inference will require fecal microbiota transplantation, depletion, and/or mono-colonization experiments to test whether *L. murinus* is necessary and/or sufficient for the observed protection. The superior efficacy of EcN-GPX4 compared with wild-type EcN suggests a possible synergy between its enzymatic antioxidant activity and its microbiota-modulating capacity. Although our current findings are based on 16S rRNA sequencing, additional studies employing metagenomics and fecal microbiota transplantation are warranted to clarify the causal role of *L. murinus* in anti-pyroptotic effects. EcN-GPX4 also inhibited intestinal NLRP3 inflammasome assembly and reduced IL-1β release, thereby complementing its pyroptosis-suppressive effects. Molecular docking simulations further suggest that GPX4 may interact directly with GSDMD, stabilizing its uncleaved form—an observation consistent with previous reports linking GPX4 deficiency to intensified ferroptosis–pyroptosis crosstalk [10, 47]. In addition, EcN-GPX4-driven metabolic reprogramming, characterized by reduced arachidonic acid metabolites and increased antioxidant levels, supports the concept that microbial metabolites can modulate host oxidative stress and inflammation [48, 49]. Nonetheless, confirmation of *L. murinus* as a direct effector strain will require single-strain colonization experiments, and additional studies are needed to elucidate the temporal relationship between microbiota remodeling and GPX4 delivery.

This study has several limitations. First, the relative contributions of bacterial-derived versus host-derived GPX4 to the observed protective phenotype remain uncertain and should be clarified using tissue-specific GPX4 knockout models. Second, the potential impact of gastric acid and bile salts on the viability of the engineered probiotic was not evaluated. Future work could address this by employing FDA approved, food-grade encapsulation materials, such as chitosan, sodium alginate, or enteric coatings to improve survival and colonization efficiency in the gastrointestinal tract. Third, although EcN-GPX4 influenced multiple ferroptosis-related metabolic pathways, its exact role in sepsis-associated ferroptosis and its mechanistic crosstalk with pyroptosis remain to be defined, for example through experimental approaches using inhibitors such as liproxstatin-1. In addition, while endotoxemia enables mechanistic d issection, polymicrobial infectious models (e.g., CLP) and post-onset dosing paradigms are essential to define therapeutic windows and to better mirror clinical sepsis heterogeneity. These will be prioritized in future work.

In summary, this work integrates microbiome engineering with oxidative stress regulation to expand available intervention options for sepsis. Utilizing a safe, engineered probiotic for localized enzyme delivery, it offers a tissue-targeted anti-inflammatory strategy that avoids systemic immunosuppression. Future research should aim to optimize GPX4 delivery kinetics and investigate combination approaches with antibiotics or immunomodulators. Ultimately, this study establishes a synthetic biology driven probiotic precision intervention platform, opening new avenues for the prevention and treatment of inflammatory diseases.

Funding

This work was supported by the National Natural Science Foundation of China (Grant Nos. 32460868, 31960692, and 31660704).

Conflict of Interest

The authors declare no conflict of interest.

Data availability

The data supporting the findings of this study are provided in the Supporting Information of this article. Additional file 1: Table S1: glk-pHCE-pelB-GPX4 sequence; Table S2: PCR primers sequences; Figure S1: Identification of the genetically engineered strain EcN-GPX4; Table S3: Molecular docking scores of GPX4 and GSDMD; Figure S1: Uncropped versions of all gel images-1 (related to Figures 2E, 3H, and 5A); Figure S2: Uncropped versions of all gel images-2 (related to Figures 7A and 8E).

Ethics approval

The present study obtained ethical approval from the Animal Ethics Committee of Yunnan Agriculture University (202303006) and conformed to the ARRIVE guidelines.

Acknowledgments

We thank all project contributors for their efforts and Ms. Hongxu Yao (Yunnan Agricultural University) for her assistance with data analysis and organization.

References

1. van der Poll T, Shankar-Hari M, Wiersinga WJ: The immunology of sepsis. *Immunity* 2021, 54(11):2450-2464.
2. Hotchkiss RS, Monneret G, Payen D: Sepsis-induced immunosuppression: from cellular dysfunctions to immunotherapy. *Nature reviews Immunology* 2013, 13(12):862-874.
3. Jarczak D, Kluge S, Nierhaus A: Sepsis-Pathophysiology and Therapeutic Concepts. *Frontiers in medicine* 2021, 8:628302.
4. Polderman KH, Girbes AR: Drug intervention trials in sepsis: divergent results. *Lancet* 2004, 363(9422):1721-1723.
5. Bai Y, Pan Y, Liu X: Mechanistic insights into gasdermin-mediated pyroptosis. *Nature Reviews Molecular Cell Biology* 2025, 26(7):501-521.
6. Rathkey JK, Zhao J, Liu Z, Chen Y, Yang J, Kondolf HC, Benson BL, Chirieleison SM, Huang AY, Dubyak GR *et al*: Chemical disruption of the pyroptotic pore-forming protein gasdermin D inhibits inflammatory cell death and sepsis. *Sci Immunol* 2018, 3(26).
7. Kayagaki N, Stowe IB, Lee BL, O'Rourke K, Anderson K, Warming S, Cuellar T, Haley B, Roose-Girma M, Phung QT *et al*: Caspase-11 cleaves gasdermin D for non-canonical inflammasome signalling. *Nature* 2015, 526(7575):666-671.

8. Vandenabeele P, Bultynck G, Savvides SN: Pore-forming proteins as drivers of membrane permeabilization in cell death pathways. *Nature Reviews Molecular Cell Biology* 2023, 24(5):312-333.
9. Wright SS, Kumari P, Fraile-Ágreda V, Wang C, Shivcharan S, Kappelhoff S, Margheritis EG, Matz A, Vasudevan SO, Rubio I *et al*: Transplantation of gasdermin pores by extracellular vesicles propagates pyroptosis to bystander cells. *Cell* 2025, 188(2):280-291.e217.
10. Kang R, Zeng L, Zhu S, Xie Y, Liu J, Wen Q, Cao L, Xie M, Ran Q, Kroemer G *et al*: Lipid Peroxidation Drives Gasdermin D-Mediated Pyroptosis in Lethal Polymicrobial Sepsis. *Cell Host Microbe* 2018, 24(1):97-108.e104.
11. Mariathasan S, Newton K, Monack DM, Vucic D, French DM, Lee WP, Roose-Girma M, Erickson S, Dixit VM: Differential activation of the inflammasome by caspase-1 adaptors ASC and Ipaf. *Nature* 2004, 430(6996):213-218.
12. Shi J, Zhao Y, Wang K, Shi X, Wang Y, Huang H, Zhuang Y, Cai T, Wang F, Shao F: Cleavage of GSDMD by inflammatory caspases determines pyroptotic cell death. *Nature* 2015, 526(7575):660-665.
13. Silva CMS, Wanderley CWS, Veras FP, Sonego F, Nascimento DC, Gonçalves AV, Martins TV, Cólon DF, Borges VF, Brauer VS *et al*: Gasdermin D inhibition prevents multiple organ dysfunction during sepsis by blocking NET formation. *Blood* 2021, 138(25):2702-2713.
14. Wang S, Ren H, Fan C, Lin Q, Liu M, Tian J: Ochratoxin A Induces Renal Cell Ferroptosis by Disrupting Iron Homeostasis and Increasing ROS. *Journal of Agricultural and Food Chemistry* 2024, 72(3):1734-1744.
15. Ajiboye TO, Komolafe YO, Oloyede OB, Ogunbode SM, Adeoye MD, Abdulsalami IO, Nurudeen QO: Polyphenolic extract of Sorghum bicolor grains enhances reactive oxygen species detoxification in N-nitrosodiethylamine-treated rats. *Food Science and Human Wellness* 2013, 2(1):39-45.
16. Shimizu J, Murao A, Nofi C, Wang P, Aziz M: Extracellular CIRP Promotes GPX4-Mediated Ferroptosis in Sepsis. *Front Immunol* 2022, 13:903859.
17. Xie Y, Kang R, Klionsky DJ, Tang D: GPX4 in cell death, autophagy, and disease. *Autophagy* 2023, 19(10):2621-2638.
18. Zhang X, Liu H, Hashimoto K, Yuan S, Zhang J: The gut-liver axis in sepsis: interaction mechanisms and therapeutic potential. *Critical care (London, England)* 2022, 26(1):213.
19. Stange EF, von Bünau R, Erhardt A: Ulcerative colitis-Maintanance of Remission With the Probiotic Escherichia coli Strain Nissle 1917. *Gastroenterology* 2021, 160(7):2632.
20. Zou ZP, Du Y, Fang TT, Zhou Y, Ye BC: Biomarker-responsive engineered probiotic diagnoses, records, and ameliorates inflammatory bowel disease in mice. *Cell Host Microbe* 2023, 31(2):199-212.e195.
21. Liu C, Lv X, Liu L, Li J, Du G, Chen J, Liu Y: Constructing an Antibiotic-Free Protein Expression System for Ovalbumin Biosynthesis in Probiotic Escherichia coli Nissle 1917. *Journal of Agricultural and Food Chemistry* 2024, 72(15):8693-8703.
22. Wang Y, Hu L, Wang L, Zhang C, Shen W, Yang H, Li M, Zhang X, Xu M, Zhang M *et al*: Engineered Escherichia coli Nissle 1917 targeted delivery of extracellular PD-L1-mFc fragment for treating inflammatory bowel disease. *Acta Pharmaceutica Sinica B* 2025.
23. Lynch JP, González-Prieto C, Reeves AZ, Bae S, Powale U, Godbole NP, Tremblay JM, Schmidt FI, Ploegh HL, Kansra V *et al*: Engineered Escherichia coli for the in situ secretion of therapeutic nanobodies in the gut. *Cell Host & Microbe* 2023, 31(4):634-649.e638.
24. Huang L, Tang W, He L, Li M, Lin X, Hu A, Huang X, Wu Z, Wu Z, Chen S *et al*: Engineered probiotic Escherichia coli elicits immediate and long-term protection against influenza A virus in mice. *Nat Commun* 2024, 15(1):6802.
25. Gurbatri CR, Radford GA, Vrbanac L, Im J, Thomas EM, Coker C, Taylor SR, Jang Y, Sivan A, Rhee K *et al*: Engineering tumor-colonizing E. coli Nissle 1917 for detection and treatment of colorectal neoplasia. *Nat Commun* 2024, 15(1):646.
26. Jiang Y, Chen B, Duan C, Sun B, Yang J, Yang S: Multigene editing in the Escherichia coli genome via the CRISPR-Cas9 system. *Appl Environ Microbiol* 2015, 81(7):2506-2514.
27. Sharan SK, Thomason LC, Kuznetsov SG, Court DL: Recombineering: a homologous recombination-based method of genetic engineering. *Nature protocols* 2009, 4(2):206-223.
28. Kayagaki N, Warming S, Lamkanfi M, Walle LV, Louie S, Dong J, Newton K, Qu Y, Liu J, Heldens S *et al*: Non-canonical inflammasome activation targets caspase-11. *Nature* 2011, 479(7371):117-121.
29. Shrum B, Anantha RV, Xu SX, Donnelly M, Haeryfar SMM, McCormick JK, Mele T: A robust scoring system to evaluate

sepsis severity in an animal model. *BMC Research Notes* 2014, 7(1):233.

30. Xiaowei W, Athanasia S, Huajun W, Brian S: PrimerBank: a PCR primer database for quantitative gene expression analysis, 2012 update. *Nucleic Acids Research* 2011.
31. Athanasia S, Xiaowei W, Huajun W, Brian S: PrimerBank: a resource of human and mouse PCR primer pairs for gene expression detection and quantification. *Nucleic Acids Research* 2009.
32. Yan Y, Tao H, He J, Huang S-Y: The HDOCK server for integrated protein–protein docking. *Nature protocols* 2020, 15(5):1829-1852.
33. Karen V S, Meng D, Jenny P-Y T: The NLRP3 inflammasome: molecular activation and regulation to therapeutics. *Nature reviews Immunology* 2019, 19(8).
34. Lieselotte VW, Mohamed L: Drugging the NLRP3 inflammasome: from signalling mechanisms to therapeutic targets. *Nature reviews Drug discovery* 2023, 23(1).
35. Mu J, Sun Q, Lin N, Yue C, Zhu J, Zou H, Zhao H, Song R, Liu Z, Ma Y: β-Hydroxybutyric Acid-Induced Bovine Endometrial Epithelial Cell Pyroptosis via Activating P2X7R. *Journal of Agricultural and Food Chemistry* 2025, 73(34):21296-21308.
36. Ingold I, Berndt C, Schmitt S, Doll S, Poschmann G, Buday K, Roveri A, Peng X, Porto Freitas F, Seibt T *et al*: Selenium Utilization by GPX4 Is Required to Prevent Hydroperoxide-Induced Ferroptosis. *Cell* 2018, 172(3):409-422.e421.
37. Jia M, Qin D, Zhao C, Chai L, Yu Z, Wang W, Tong L, Lv L, Wang Y, Rehwinkel J *et al*: Redox homeostasis maintained by GPX4 facilitates STING activation. *Nat Immunol* 2020, 21(7):727-735.
38. Woo MS, Mayer C, Binkle-Ladisch L, Sonner JK, Rosenkranz SC, Shaposhnykov A, Rothammer N, Tsvilovskyy V, Lorenz SM, Raich L *et al*: STING orchestrates the neuronal inflammatory stress response in multiple sclerosis. *Cell* 2024, 187(15):4043-4060.e4030.
39. Bongers KS, Chanderraj R, Woods RJ, McDonald RA, Adame MD, Falkowski NR, Brown CA, Baker JM, Winner KM, Fergle DJ *et al*: The Gut Microbiome Modulates Body Temperature Both in Sepsis and Health. *Am J Respir Crit Care Med* 2023, 207(8):1030-1041.
40. Gong S, Yan Z, Liu Z, Niu M, Fang H, Li N, Huang C, Li L, Chen G, Luo H *et al*: Intestinal Microbiota Mediates the Susceptibility to Polymicrobial Sepsis-Induced Liver Injury by Granisetron Generation in Mice. *Hepatology* 2019, 69(4):1751-1767.
41. R H, N D, Y H, X W, Y X, X Q, X S, T B, Y X, X Z *et al*: Ligilactobacillus Murinus and Lactobacillus Johnsonii Suppress Macrophage Pyroptosis in Atherosclerosis through Butyrate-GPR109A-GSDMD Axis. *Advanced science (Weinheim, Baden-Wurttemberg, Germany)* 2025, null:e01707.
42. Chuandong Z, Hu J, Li J, Wu Y, Wu C, Lai G, Shen H, Wu F, Tao C, Liu S *et al*: Distribution and roles of Ligilactobacillus murinus in hosts. *Microbiological Research* 2024, 282:127648.
43. Zhong Z, Umemura A, Sanchez-Lopez E, Liang S, Shalapour S, Wong J, He F, Boassa D, Perkins G, Ali SR *et al*: NF-κB Restricts Inflammasome Activation via Elimination of Damaged Mitochondria. *Cell* 2016, 164(5):896-910.
44. S C, Y X, D G, T L, Z T, X R, X W: Effects of Salmonella Typhimurium infection on intestinal flora and intestinal tissue arachidonic acid metabolism in Wenchang chickens. *Frontiers in microbiology* 2025, 16:1514115.
45. Ichihara G, Katsumata Y, Sugiura Y, Matsuoka Y, Maeda R, Endo J, Anzai A, Shirakawa K, Moriyama H, Kitakata H *et al*: MRP1-Dependent Extracellular Release of Glutathione Induces Cardiomyocyte Ferroptosis After Ischemia-Reperfusion. *Circ Res* 2023, 133(10):861-876.
46. Yan-Yu Z, Yun-Da Y, Fang C, Xin G, Jun-Li K, Yu-Feng H, Fan H, Yan D, Ying X, Peng W *et al*: (9S,13R)-12-oxo-phytodienoic acid attenuates inflammation by inhibiting mPGES-1 and modulating macrophage polarization via NF-κB and Nrf2/HO-1 pathways. *Pharmacol Res* 2022, 182(0).
47. Lu ZX, Liu LX, Fu Z, Wang SN, Sun CN, Yu WG, Lu XZ: Chitosan oligosaccharides alleviate macrophage pyroptosis and protect sepsis mice via activating the Nrf2/GPX4 pathway. *Int J Biol Macromol* 2024, 277(Pt 1):133899.
48. F DV, A DG, V P, LR L, F S: Gut microbiota, intestinal permeability, and systemic inflammation: a narrative review. *Internal and emergency medicine* 2024, 19(2):275-293.
49. Z Z, Y Y, X Z, F D, S C, X T: Ameliorative Effects of Lactobacillus paracasei L14 on Oxidative Stress and Gut Microbiota in Type 2 Diabetes Mellitus Rats. *Antioxidants (Basel, Switzerland)* 2023, 12(8).